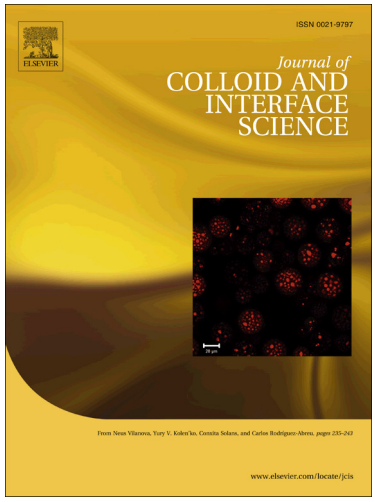


# Antibacterial potential of electrochemically exfoliated graphene sheets

Zoran M. Marković, Danka M. Matijašević, Vladimir B. Pavlović, Svetlana P. Jovanović, Ivanka D. Holclajtner-Antunović, Zdenko Špitalský, Matej Mičušik, Miroslav D. Dramićanin, Dušan D. Milivojević, Miomir P. Nikšić, Biljana M. Todorović Marković

PII: S0021-9797(17)30377-6
DOI: http://dx.doi.org/10.1016/j.jcis.2017.03.110
Reference: YJCIS 22207

To appear in: *Journal of Colloid and Interface Science*

Received Date: 2 February 2017
Revised Date: 28 March 2017
Accepted Date: 28 March 2017

Please cite this article as: Z.M. Marković, D.M. Matijašević, V.B. Pavlović, S.P. Jovanović, I.D. Holclajtner-Antunović, Z. Špitalský, M. Mičušik, M.D. Dramićanin, D.D. Milivojević, M.P. Nikšić, B.M. Todorović Marković, Antibacterial potential of electrochemically exfoliated graphene sheets, *Journal of Colloid and Interface Science* (2017), doi: http://dx.doi.org/10.1016/j.jcis.2017.03.110

# Antibacterial potential of electrochemically exfoliated graphene sheets

Zoran M. Marković [1]*, Danka M. Matijašević[4], Vladimir B. Pavlović[4], Svetlana P. Jovanović[2], Ivanka D. Holclajtner-Antunović[4], Zdenko Špitalský[1], Matej Mičušik[1], Miroslav D. Dramićanin[2], Dušan D. Milivojević[2], Miomir P. Nikšić[4], Biljana M. Todorović Marković[2]*

[1]Polymer Institute, Slovak Academy of Sciences, Dubravska cesta 9, 84541 Bratislava, Slovakia

[2]Vinča Institute of Nuclear Sciences, University of Belgrade, P.O.B. 522, 11001 Belgrade, Serbia

[3]Faculty of Physical Chemistry, University of Belgrade, Studentski trg 12-16, 11158 Belgrade, Serbia

[4]Faculty of Agriculture, University of Belgrade, Nemanjina 6, 11080 Belgrade-Zemun, Serbia

Abstract

Electrochemically exfoliated graphene is functionalized graphene with potential application in biomedicine. Two most relevant biological features of this material are its electrical conductivity and excellent water dispersibility. In this study we have tried to establish the correlation between graphene structure and its antibacterial properties. The exfoliation process was performed in a two electrode-highly oriented pyrolytic graphite electrochemical cell. Solution of ammonium persulfate was used as an electrolyte. Exfoliated graphene sheets were dispersed in aqueous

* Corresponding authors: Tel: +421-2-3229 4326. Email addresses: zm25101967@yahoo.com, zoran.markovic@savba.sk (Z. Markovi ), biljatod@vin.bg.ac.rs (B. Todorovi -Markovi )

media and characterized by atomic force microscopy, scanning electron microscopy, Raman spectroscopy, Fourier transform infrared spectroscopy, X photoelectron spectroscopy, X-ray diffraction, electron paramagnetic resonance, zeta potential, contact angle measurements and surface energy. Antibacterial assays have shown lack of the significant antibacterial activity. Major effect on bacteria was slight change of bacteria morphology. Membrane remained intact despite significant change of chemical content of membrane components.

Keywords: exfoliated graphene; antibacterial tests; scanning electron microscopy; atomic force microscopy; X-photoelectron spectroscopy

## 1.Introduction

Graphene presents one atom thick layer of carbon atoms that are perfectly arranged in a two-dimensional honeycomb lattice. Due to its unique properties especially electrical this material is the object of investigation of many researchers [1–5]. On the other side, graphene oxide (GO) is a single sheet of functionalized graphene that does not conduct electricity but is fully dispersible in water. In this way, graphene oxide is plausible candidate for biomedical applications [6]. Among these two extremes, the third type of graphene is positioned similar to reduced graphene oxide [7]. Electrochemically exfoliated graphene is electrically conducting and excellent water dispersible. It is functionalized at the edges with carboxyl and hydroxyl groups. Sheet core is similar to pristine graphene with elevated level of defects [8, 9].

Many production methods such as chemical vapour deposition or epitaxial growth are applied for graphene synthesis [10–12]. GO is commonly produced by Hummers reaction based on graphite treatment with concentrated sulphuric acid in the presence of strong oxidizers [13]. One of the promising methods for massive production of conductive and water dispersible graphene is

electrochemical exfoliation which presents cost-effective and green approach in graphene synthesis [14–17]. By applying this method, graphite is exfoliated into graphene sheets in a convenient way, preserving their conjugated honeycomb structure. To do this, the non-covalent, weak but significant interactions presented between graphene sheets should be overcome. Electrochemical exfoliation takes place in different electrolyte surroundings: diluted sulphuric acid or potassium persulfate [14, 18]. As a carbon source it can be used different carbon materials: graphite rods, graphite foils or highly oriented pyrolytic graphite (HOPG) [19].

Few-layer (FLG) or multi-layer graphene (MLG) consists of a small number (between two and approximately 10) of well-defined, countable, stacked graphene layers of extended lateral dimension either as a free-standing flake or a substrate-bound coating [20]. Single layer graphene (SLG) consists only of one layer that can be distuingushed from FLG by Raman spectroscopy [21]. Basic feature of SLG or FLG is a huge surface to volume ratio which is easily expressed by aspect ratio diameter/height. Typical aspect ratio of graphene based materials is below 1000 [22].

There is a great interest in producing graphene modified surfaces for antibacterial applications. Studies have suggested that such surfaces are indeed antibacterial [23, 24]. A recent published study claims that antibacterial activity of graphene film does not stem from reactive oxygen species (ROS) mediated damage, but through electron transfer interaction from microbial membrane to graphene [25]. GO coated with bovine serum albumin (BSA) protein or tryptophan loses antibacterial activity [26]. GO is reduced to conductive graphene oxide by metabolic activity of the surviving bacteria through their glycolysis process [27]. Sheet resistivity of GO was decreased two orders of magnitude after 48 hours exposure to microbes. The antibacterial activity of GO sheets toward *Escherichia coli* cells is lateral size dependent [28]. Larger GO sheets show stronger antibacterial activity than do smaller ones. Antibacterial tests show that all

GO-containing cotton fabrics possess strong antibacterial property and could inactivate 98% of bacteria [29]. Most significantly, these fabrics can still kill more than 90 % bacteria even after being washed for 100 times. Another mechanism for graphene antibacterial activity is photothermal. In a recent study, Wu et al. synthesized graphene-based photothermal agent for the efficient capture and killing of both gram-positive *Staphylococcus aureus* and gram-negative (*E. coli*) bacteria upon near-infrared (NIR) laser irradiation [30]. However, some authors reported that GO stimulate the growth of bacteria [31] or that sulfur impurities remained after GO synthesis determine its antibacterial activity [32].

Many parameters may affect the graphene antibacterial properties: sheet size and concentration, surface area, surface roughness, hydrophilicity, dispersibility and functionalization [33]. There is the difference among interactions of bacteria and graphene based materials in terms of the shape of graphene (graphene paper, graphene thin films, graphene composites and graphene colloids). Membrane rupture was proposed to be the toxicity mechanism of colloidal graphene. In colloids, the orientation of the graphene particles may interact with bacteria in a manner of egdewise contact [34].

In this paper we have used highly oriented pyrolytic graphite as a carbon source, and performed detailed properties analysis of exfoliated graphene sheets. Numerous characterization techniques have been used to investigate structural, spectroscopical and antibacterial properties of exfoliated graphene: atomic force microscopy (AFM), scanning electron microscopy (SEM), Raman, X-photo electron (XPS) and Fourier transform infrared spectroscopy (FTIR), X-ray diffraction (XRD), electron paramagnetic resonance (EPR), zeta potential, contact angle measurements surface energy and antibacterial tests.

## 2. Experimental procedure

### 2.1. Preparation of graphene dispersion and graphene thin films

Electrochemical exfoliation of graphite was performed in the two-electrode system dipped in electrolyte (ammonium persulfate-purchased from Sigma Aldrich). As a graphite electrode, HOPG (produced in Vinča Institute of Nuclear Sciences) was used. As a counter electrode platinum was used. Applied direct current voltage were +3 and +12 V. Electrolyte solution was prepared by dissolving $(NH_4)_2SO_4$ in water (concentration of 0.1 M). Depending on the applied voltage exfoliation process lasted from 5 min to 24 hours. The weight of exfoliated product was 12 g per day. Exfoliated powder was washed with 5 L of MilliQ water using coarse filter paper with pore size of 15 microns. In this step both ammonium persulfate (APS) and small size graphene flakes were washed. This obtained powder was dispersed in aqueous media by ultrasonication for 5 minutes. Aqueous dispersion of graphene sheets was allowed to settle down for 2 days. Then this dispersion was centrifuged at 6500 rpm for 30 min.

Supernatant was used as dispersion, for deposition of thin films, thin film characterization and antibacterial tests. Thin films were deposited by vacuum filtration on ano-disc inorganic membranes with pore size of 200 nm and diameter 25mm (Whatman filters). Deposited graphene thin films were transferred to glass substrate. Graphene thin films deposited on ano-discs have been transferred to glass substrates by the following way: Ano-disc with graphene thin film was etched in 50 ml of 0.5M NaOH water solution for two hours. After etching, transparent graphene thin film floated on water surface. Half liter of water was added in solution gently to reduce NaOH concentration. Glass substrate was carefully dipped in water, translated below graphene film, slowly elevated and extracted from water. Further in the text, HOPG sample exfoliated at

+3 V was denoted as the EHOPG3 whereas that exfoliated at +12 V was denoted as the EHOPG12.

2.2. Characterization of graphene dispersion and graphene thin films

Microstructure and morphology of the EHOPG3 and EHOPG12 thin films deposited on glass substrate were recorded by SEM (JEOL JSM-6390LV) and AFM (Quesant, Ambious Technology, USA). The lateral dimensions of EHOPG3 and EHOPG12 sheets were determined by SEM software. The AFM was operated in tapping mode at room temperature [35]. The AFM measurements were performed in air using a silicon T-shaped cantilever with a spring constant of 40 N/m on square areas of 1 μm × 1 μm. All images were obtained at 1 Hz, with a 512 × 512 image resolution over different square areas. Gwyddion software was used to measure lateral and height size of the EHOPG sheets as well as for determination of surface roughness- root-mean square roughness (RMS) [36].

XPS of the EHOPG3 and EHOPG12 thin films were performed using a Thermo Scientific K-Alpha XPS system (Thermo Fisher Scientific, UK) equipped with a micro-focused, monochromatic Al Kα X-ray source (1486.6 eV). An X-ray beam of 400 mm in size was used at 6 mA x 12 kV. The spectra were acquired in the constant analyzer energy mode with pass energy of 200 eV for the survey. Narrow regions were collected with pass energy of 50 eV. Charge compensation was achieved with the system flood gun that provides low energy electrons (~0 eV) and low energy argon ions (20 eV) from a single source. Thermo Scientific Avantage software, version 5.952 (Thermo Fisher Scientific), was used for the digital acquisition and data processing. Spectral calibration was determined by using the automated calibration routine and the internal Au, Ag and Cu standards supplied with the K-Alpha system.

The surface composition (in atomic %) was determined by considering the integrated peak areas of the detected atoms and their respective sensitivity factors. The fractional concentration of a particular element A was computed using:

$$\%\,A = \frac{I_A/s_A}{\sum(I_n/s_n)} \times 100\% \quad (1)$$

where $I_n$ and $s_n$ are the integrated peak areas and the Scofield sensitivity factors corrected for the analyzer transmission, respectively.

Zeta potential (ζ-potential) of the EHOPG3 and EHOPG12 dispersions were assessed by DLS using Zetasizer Nano-ZS (Malvern Instruments, UK) equipped with a 4 mW helium/neon laser (λ = 633 nm) and thermo-electric temperature controller, with the following parameters set for graphene colloidal particles: refractive index = 2.67, absorption = 0.01, and viscosity = 0.89 cP. All measurements were performed at 25 °C. Value of zeta potential was averaged from five measurements.

Contact angle measurements were carried out by using the sessile drop method [37]. The contact angle data of the EHOPG3 and EHOPG12 thin films on glass were obtained by the Surface Energy Evaluation System (SEE System; Advex Instruments, Czech Republic). Deionized water, ethylene glycol and diiodomethane were used as the testing liquids. The droplets volume was set to 5 μL for all experiments to avoid errors connected with the gravity acting to the sessile drop. The contact angle is usually measured by the tangent at the three phase interface (solid-liquid-vapor [38]. The liquid drop of 5 μL was placed onto the surface of the EHOPG3 and EHOPG12 thin films with the help of micro syringe. The image of liquid is directly projected on the screen. The screen has two calibrated axes mutually perpendicular to each other, which can be rotated. All of the calculations were made by the SEE System software for analysis. Six contact angle

readings were averaged to obtain one representative value. The substrate surface free energy was evaluated using these data by Lifshitz–Van der Waals "acid–base" model. Contact angle was measured immediately after thin film deposition.

FTIR spectra of the EHOPG3 and EHOPG12 thin films were measured at room temperature in the spectral range from 400 to 4000 $cm^{-1}$ on a Nicollet 380 FT-IR, Thermo Electron Corporation spectrometer operating in ATR mode.

XRD patterns of the EHOPG3 and EHOPG12 powder samples were measured using a Rigaku Smart Lab diffractometer in a 2θ range from 5° to 70° and were counted at 0.7°/min in 0.1° steps.

Raman spectra of the EHOPG3 and EHOPG12 thin films were obtained by DXR Raman microscope (Thermo Scientific) using 532 nm excitation lines with power of 5 mW. The spectral resolution was 1 $cm^{-1}$. Acquisition time was 10 × 10 s. Raman spectra were recorded at room temperature.

Electron Paramagnetic Resonance (EPR) analyses of EHOPG3 and EHOPG12 dispersions were performed at room temperature using a EPR Spectrometer MiniScope 300, Magnettech, Berlin, Germany, operating at a nominal frequency of 9.5 GHz. The microwave power was 1 mW (microwave attenuation of 20 dB), with a modulation amplitude of 0.2 mT. UV irradiation was performed within the EPR resonator, through irradiation window, using Hamamatsu LC8 spot light source, typeL9566-01, radiant wavelength range (300–450 nm).

The formation of singlet oxygen ($^1O_2$) was followed by specific reaction between $^1O_2$ and 2,2,6,6-tetramethylpiperidine (TEMP) in which a stable radical adduct, TEMP-$^1O_2$ (or TEMPO) was formed. The EHOPG3 and EHOPG12 dispersions, in concentration of 0.2 wt. %, were

mixed with TEMP (at a final concentration of 30 mM). Prepared mixtures were air-saturated before EPR measurement. All three mixtures were measured before and during light exposure. These mixtures were exposed to UV-Vis light ($\lambda > 300$ nm) for 10 minutes.

The ability of dispersions to produce hydroxyl ($HO^{\bullet}$) and superoxide ($O_2^{-\bullet}$) radicals was studied using 5,5-dimethyl-1-pyrroline-N-oxide (DMPO) as a spin trap for both of these radical species. For EPR measurements, we prepared mixtures of DMPO, in final concentration of 100 mM and sample, where concentration of material was 0.5 mg $mL^{-1}$.

2.3. Bacteria strains and culture conditions

The antibacterial activity of the EHOPG3 and EHOPG12 dispersions was performed against *Escherichia coli* ATCC 25922 and *Staphylococcus aureus* ATCC 25923. Selected species of bacteria originate from ATCC (American Type Culture Collection, Rockville, Maryland). The cultivation/assay medium for tested bacteria strains was Müeller Hinton Broth (MHB) /Agar (MHA) (HiMedia Laboratories, India). Concentrations of approximately $10^5$–$10^6$ CFU $mL^{-1}$ were prepared from overnight broth culture of test strain and used for the antibacterial activity assays.

2.4. Effect of EHOPG3 and EHOPG12 on cell growth monitored by measuring optical density (OD)

EHOPG3 and EHOPG12 stock solution of 1 mg $mL^{-1}$ was sterilized by gamma irradiation at a dose of 10 kGy and used to examine the kinetics of bacterial growth using 96-well plates. The pH of prepared colloids was adjusted to value 7. The wells of the microtiter plates, filled with 100 µL of two-fold serially diluted samples in water, were then inoculated with 100 µL of the bacterial suspension. Concentrations of the EHOPG3 and EHOPG12 ranged from 0.125 to 0.5 mg $mL^{-1}$. Negative controls were wells with growth medium and EHOPG3 or EHOPG12, while

MH broth with the tested bacteria served as positive controls. The microplate reader (ELx808, BioTek Instruments, Inc., USA) controlled by Gen5TM Software was used to monitor the cell growth by measuring the turbidity $OD_{630}$ (optical density at 630 nm) at 60 min intervals during 24 h. OD630 is a method used to determine the amount of light scattered by the bacteria rather than the amount of light absorbed and is proportional to the cell density [39]. Plate was shaken for 10 s before every reading. The $OD_{630}$ was corrected for OD of negative control at the same point of measurement.

2.5. Bacteria growth in the presence of EHOPG3 and EHOPG12 determined by viable count

Bacteria growth in the presence of EHOPG3 and EHOPG12 was determined by macrodilution method, according to Klačnik et al. [40] with slight modification. EHOPG3 and EHOPG12 were diluted in 1 mL of bacterial culture to reach the concentration of 0.5 mg $mL^{-1}$. This concentration was chosen according to the results of previous assay. The viable count of tested bacteria was determined by taking samples at the initial point (0 h) and after 3, 6, 9 and 24 h and plating out the aliquot (10 µL) on MHA after serial sample dilutions. The plates were incubated under aerobic conditions; at 37 °C for 24 h. Positive controls were prepared in the same manner, except without adding the EHOPG3 or EHOPG12. The number of the tested bacteria (expressed as log10 CFU $mL^{-1}$) was calculated by taking into account dilution of the samples and the amount plated out on the MHA. All experiments were performed in triplicates and the mean log CFU $mL^{-1}$ as well as the standard deviations was calculated.

2.6. Loss of 260-nm-absorbing material

The extracellular 260-nm-absorbing material released by the cells was determined using slightly modified method described by Carson et al. [41]. Bacterial suspensions (pretreatment sample) of approximately $10^5$–$10^6$ CFU $mL^{-1}$ were taken, diluted in a ratio 1:100, and filtered

through a 0.22-µm pore size filter (Sartorius, Germany). The EHOPG3 and EHOPG12 were added in 1 mL of *S. aureus* or *E. coli* suspensions to reach final concentration of 0.5 mg $mL^{-1}$. Cells without samples were used as a control. All the samples were incubated at 37 ºC, and additional aliquots of control and treated cell suspensions were removed after 4 and 8 h, diluted and filtered as described above. The release of UV-absorbing material was measured using a Shimadzu UV-1800 UV-VIS Spectrophotometer. The obtained results of the measurements at 260 nm at each time were expressed as a proportion of the initial optical density 260 ($OD_{260}$) value. An $OD_{260}$ is defined as the amount of light at a 260 nm wavelength which will be absorbed by an oligo if it is resuspended in 1 mL water and the concentration is read in a 1 cm quartz cuvette. The assay was carried out in triplicates.

2.7. Effect of EHOPG3 and EHOPG12 on cell growth visualized by SEM

Visualization of interactions between the EHOPG3 and EHOPG12 and bacterial strains was performed using scanning electron microscopy (SEM- JEOL JSM-6390LV) in vacuum with 10 kV acceleration voltage. Examination of the morphological changes of the bacterial cells was performed according to a slightly optimized version of the procedure described by Tyagi et al. [42]. Bacterial suspensions of approximately $10^5$–$10^6$ CFU $mL^{-1}$ were treated with EHOPG3 and EHOPG12 at the concentration of 0.5 mg $mL^{-1}$ or left untreated as the control. These suspensions were incubated for an additional 8 h at 37 ºC, harvested by centrifugation (6000 rpm, 10 min at 4 ºC) and fixed with 2.5 % glutaraldehyde over night at 4 ºC. The obtained cell pellets were washed three times with 0.1 M sodium phosphate buffer (pH 7.2) and dehydrated with graded ethanol series 25 %, 50 %, 75 %, 90 % and 2 x 100 %, 15 min each. The dehydrated samples were air dried immediately, followed by smearing on SEM stubs. All prepared samples of bacterial strains (treated with exfoliated sheets and controls) were gold-covered by a Baltec scd

005 sputter coater accessories and recorded at room temperature. The samples are denoted as the following: *E. coli* control-ECC, *S. aureus* control-SAC, treated with EHOPG3-ECEHOPG3 and SAEHOPG3, treated with EHOPG12- ECEHOPG12 and SAEHOPG12, respectively. Samples elementary composition was obtained with energy dispersive spectroscopy (EDS, Oxford Aztec X-max). The scanned surface area was 10x10 $\mu m^2$.

## 3. RESULTS AND DISCUSSION

### 3.1. Surface morphology of EHOPG

Surface morphology of EHOPG sheets prior sonification (Figs. 1(a, b)) and EHOPG3, EHOPG12 thin films was visualized by SEM and AFM-Figs. 1 (c–f). Colloidal particles of EHOPG3 and EHOPG12 have average lateral dimensions of 23.5 and 12 µm and surface roughnesses (root-mean square-rms) of colloidal particles EHOPG3 and EHOPG12 are 29.2 and 25.4 nm, respectively.

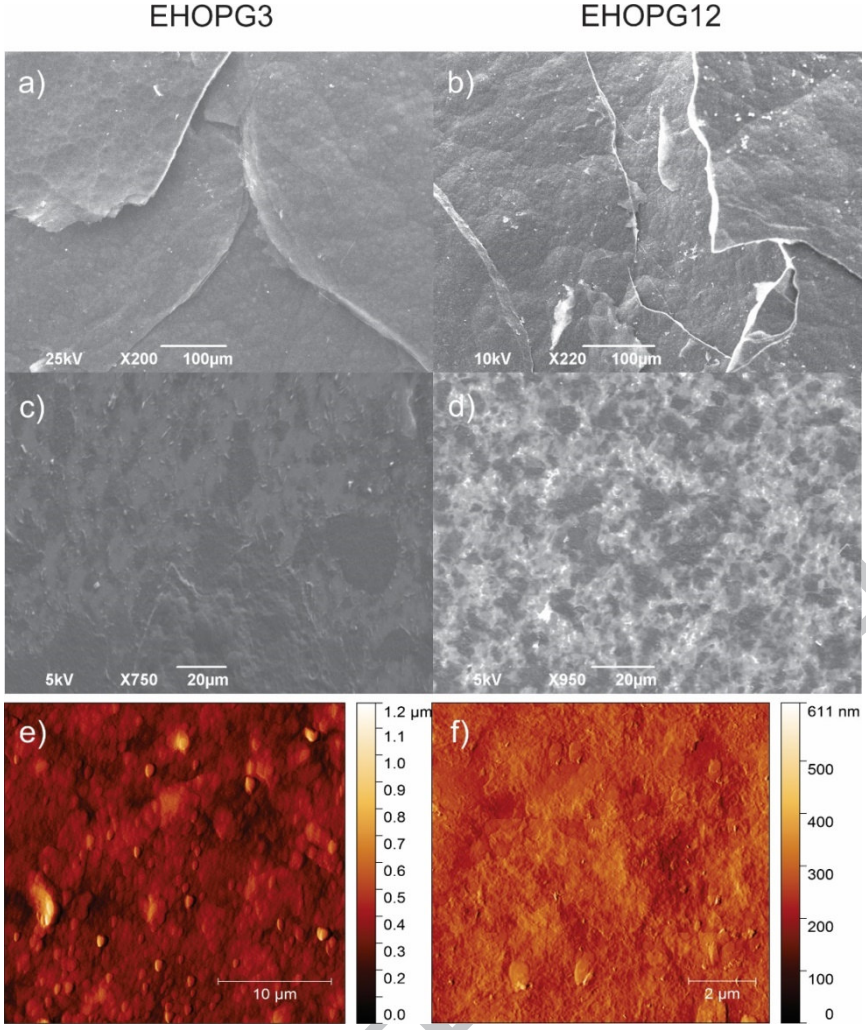


Fig. 1. SEM micrographs of: a) the EHOPG3, b) the EHOPG12, c) the EHOPG3 thin films, d) the EHOPG12 thin films, and top view AFM images of e) the EHOPG3 thin films, f) the EHOPG12 thin films.

3.2. XPS analysis of pristine and exfoliated HOPG

Fig. 2 shows the fitted XPS spectra of the HOPG, EHOPG3 and EHOPG12 samples. After the deconvolution of the C1s peak, the presence of the following carbon bonds is established: $sp^2$, $sp^3$, C-O, C=O, O-C=O and $\pi$-$\pi^*$ - Figs. 2 (a, b, c). Tables 1 and 2 present the contents of the

elements in an atomic percentage (At %) and the values of the characteristic bonds detected in all samples.

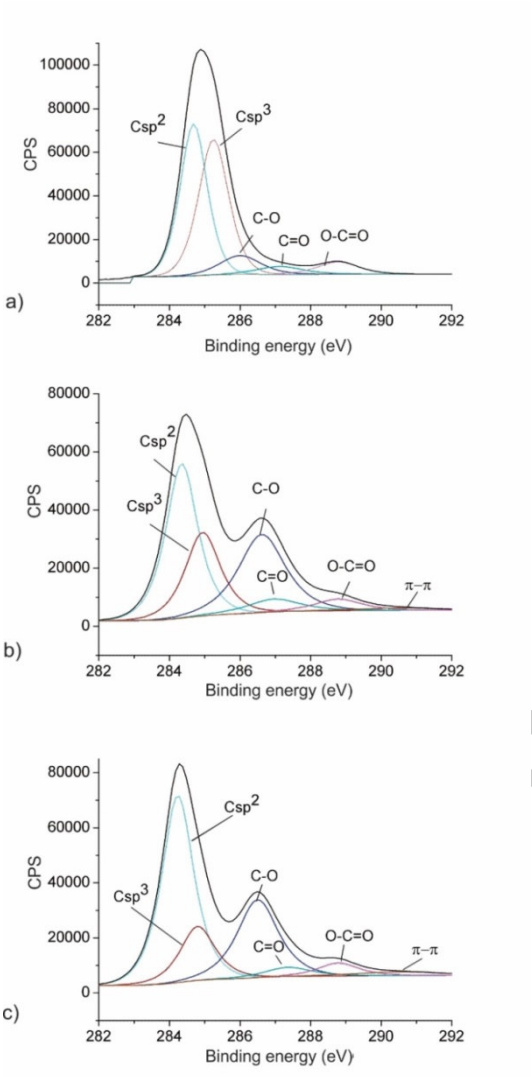


Fig. 2. The fitted XPS spectra of the HOPG (a), EHOPG3 (b) and EHOPG12 (c) samples.

The content of oxygen increases twice in the EHOPG3 and EHOPG12 samples. C/O ratios for the EHOPG3 and EHOPG12 are 3.33 and 2.87, respectively. For the EHOPG12 sample, the content of nitrogen is almost twice higher, whereas the content of sulfur is almost four times higher compared to the EHOPG3.

Data from Table 2 show that the content of $sp^2$ bonds decreases in the EHOPG3 sample compared to the starting material whereas the content of $sp^2$ bonds increases in the EHOPG12 sample. The content of $sp^3$ bonds decreases in the EHOPG3 and EHOPG12 almost 1.8 and 2.7 times compared to HOPG sample. In all the samples the carbon atoms are mainly attached to oxygen via single C-O bonds.

Table 1. XPS data of the elements detected in the HOPG, EHOPG3 and EHOPG12 samples (At %).

| Name | HOPG | EHOPG3 | EHOPG12 |
|---|---|---|---|
| C1s | 87.9 | 74.3 | 70.7 |
| O1s | 11.1 | 22.3 | 24.6 |
| N1s(C-N/$N^+$) | 1.1 | 1.4 (0.2/1.2) | 2.4 (0.3/2.1) |
| S2p | / | 0.6 | 2.3 |

Table 2. XPS data of the characteristic bonds detected in the HOPG, EHOPG3 and EHOPG12 samples (At %).

| Name | Binding energy (eV) | HOPG | EHOPG3 | EHOPG12 |
|---|---|---|---|---|
| C1s $sp^2$ | 284.38 | 42.0 | 38.2 | 48.5 |

| | | | | |
|---|---|---|---|---|
| C1s $sp^3$ | 284.98 | 41.4 | 22.6 | 15.3 |
| C1s C-O | 286.08 | 7.8 | 28.2 | 25.8 |
| C1s C=O | 286.88 | 3.7 | 5.3 | 3.5 |
| C1sO-C=O | 288.78 | 5.1 | 4.2 | 4.3 |
| C1s π-π* | 290.48 | 0.0 | 1.5 | 2.7 |

The XPS results showed that during electrochemical exfoliation of HOPG, a very strong oxidation of the EHOPG sheets occurred. The efficient intercalation of sulfate ions and the electrochemical oxidation result in a large number of functional groups attached to the surfaces and edges of the basal planes of the EHOPG3 and EHOPG12 samples. The sulfate ions intercalation between graphene sheets is confirmed by the presence of the S2p peak centered at ~ 169 eV corresponding to sulfates/sulfonates [43]. The presence of nitrogen in the EHOPG3 and EHOPG12 samples is verified by a peak centered at 401.5 eV corresponding to C-$NH_3^+$/$NH_4^+$ [44]. As we can see from Table 1 the amount of quaternized ammonium is very similar to the amount of sulfate indicating some interaction between these two groups in the EHOPG12 sample whereas the contents of nitrogen and sulfur differ for 2.33. We suppose that the presence of ammonium is a consequence of the APS that remained on the surface or between layers. As can be seen from Table 2, the content of C-O bonds increases 3.61 and 3.31 times for the EHOPG3 and EHOPG12 samples respectively compared to the HOPG sample whereas the content of C=O bonds increases 1.43 times for EHOPG3 sample and for the EHOPG12 sample remains almost the same.

The oxygen functional groups in the basal plane of EHOPG sheets are epoxy and hydroxyl, and the edges can bear carboxyls, anhydrates, lactones, phenols, lactols, pyrones, and ketones [19]. According to XPS analysis, the basal plane and edges of the larger EHOPG3 graphene sheets contain slightly more oxygen functional groups than EHOPG12 sheets.

3.3. Zeta potential and surface energy of EHOPG

Zeta potential is an important factor for characterizing the stability of dispersions. We have measured zeta potentials of the EHOPG3 and EHOPG12 dispersions. Zeta potentials are –41.61 mV and –30 mV for the EHOPG3 and EHOPG12, respectively. Standard deviations of zeta potentials of the measured samples were ± 1mV. Value of pH of aqueous colloids was 7. The measured values of zeta potentials indicate that dispersions are stabilized electrostatically and have shown good stability. There is no sign of coagulation of graphene sheets after more than two months. Both dispersions of EHOPG sheets are negatively charged. When the pH of exfoliated graphene sheets colloids was raised up to 14, zeta potentials of colloids are –52.1mV and –41 mV, respectively. In the acid environment both dispersions become unstable. Therefore, zeta potentials of EHOPG dispersions are pH dependent, which is consistent with the fact that the ionization of carboxylic acid groups is strongly related to pH.

Contact angles of the EHOPG3 and EHOPG12 samples were $77.5^{o}$±2.3 and $49.4^{o}$±3.9 respectively. This result indicates higher hydrophobicity of the EHOPG3 sample compared to the EHOPG12 sample. Surface energy of the EHOPG3 is 37.2 mJ/m$^2$ whereas of the EHOPG12 is 40.8 mJ/m$^2$. Surface free energy of several oral bacteria is nearly 100 mJ/m$^2$, i.e. almost three times higher than graphene colloidal particles [45].

3.4. FTIR Spectroscopy of EHOPG

The attenuated total reflectance (ATR) FTIR spectra of the as-deposited EHOPG3 and EHOPG12 thin films are presented in Fig. 3a (curves 1 and 2). The FTIR-ATR spectra of both material show two small peaks at 2830 and 2920 $cm^{-1}$ which stem from C-H stretching vibrations. The peaks at 1600 and 2170 $cm^{-1}$ indicate skeletal vibrations from un-oxidized graphitic domains. The peaks at 1990 and 1720 $cm^{-1}$ indicate the presence of C=O stretching vibrations while the peaks at 1420 and 1050 $cm^{-1}$ stem from C-O stretching vibrations and can be observed in the both EHOPG samples. The peaks at 985 and 1020 $cm^{-1}$ stem from free sulfate ions and can be observed in the both EHOPG samples.



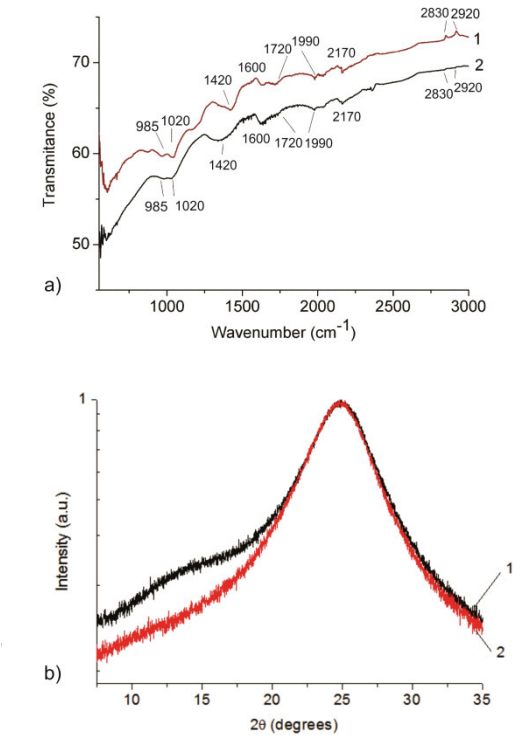


Fig. 3. a) FTIR-ATR spectra of the EHOPG3 (curve-1) and the EHOPG12 (curve-2) thin films; b) XRD patterns of the EHOPG3 (curve 1) and the EHOPG12 (curve 2).

3.5. Determination of the number of graphene layers

Quite often in the literature authors use TEM micrographs to determine the thickness of few layer graphene. However for reliable determination of few layer graphene dimensions, approximately 2000 particles used to be analyzed to get the error below 5 % [46]. XRD is much more accurate technique for determination of few layer graphene dimensions than TEM imaging.

The XRD analysis was used to determine the number of graphene layers in the exfoliated materials. The mean crystallite size (D) was calculated from the full width at half maximum (FWHM) of the XRD peak, using the Debye-Scherrer equation [18]. The interlayer distance (d) was found using the Bragg equation [47]. The average number of graphene layers was obtained by division of the mean crystallite size and the interlayer distance. Table 3 presents the number of layers (n) and the interlayer distance for the precursors and EHOPG samples obtained by fitting of XRD spectra by two Gaussians. By fitting it was established that the EHOPG3 consists of two fractions with different number of layers: 2 and 5. As for the EHOPG12 sample, it also consists of two fractions with number of layers: 9 and 16.

XRD pattern of the EHOPG3 consists of two dominant peaks at 14.28° and 24.94°. Despite severe oxidation at +12 V, the EHOPG12 sample does not contain graphene oxide peak at $2\theta \approx 11°$. The XRD pattern of this sample (Fig. 3b-curve 2) shows a broad peak at 24.79° with corresponding d-distances of 0.373 nm.

The average number of layers was reduced by one order of magnitude. The interlayer spacing has increased by 2 and 2.5 % for EHOPG3 and EHOPG12, respectively.

Table 3. Number of layers (n) and the interlayer distance (d) of the HOPG, EHOPG3 and EHOPG12.

| | n | d (nm) | n | d(nm) |
|---|---|---|---|---|
| HOPG | 99 | 0.348 | - | - |
| EHOPG3 | 2 | 0.619 | 5 | 0.368 |
| EHOPG12 | 9 | 0.373 | 16 | 0.367 |

3.6. Raman spectroscopy of pristine and exfoliated HOPG

Fig. 4a presents Raman spectra of graphene thin films of HOPG, EHOPG3 and EHOPG12 respectively. In this figure we can observed three characteristic features of Raman spectrum of graphene (G peak which origin from in-plane vibrations of $sp^2$ carbon atoms- 1580 $cm^{-1}$, D peak which origin from incorporated defects during electrochemical exfoliation-1350 $cm^{-1}$ and 2D peak-2700 $cm^{-1}$ which presents second harmonic of D peak) [48]. The D peak in the Raman spectrum of HOPG (curve 1) is very small and indicates very low number of incorporated defects in the pristine sample [49].

Figs. 4b, c and d present the fitted Raman spectra of G band of HOPG and graphene thin films of EHOPG3 and EHOPG12, respectively. G peak is fitted to four Lorentzian (1550, 1580, 1600 and 1617 $cm^{-1}$) peaks. Peaks at 1580 $cm^{-1}$, 1600 $cm^{-1}$ and 1617 $cm^{-1}$ were denoted as P1, P2 and P3. The P1 and P2 peaks are attributed to two different $E_{2g}$ vibrations due to the C-C stretching mode of atoms composing the sheets in bulk graphite and atoms in the sheets adjacent to the intercalated layer. P1 is due to inner, non-intercalated graphite layer while P2 is due to the bounding graphite layers. P1 peak is upshifted from 1580 to 1598 $cm^{-1}$ for sample exfoliated from EHOPG3 and from 1580 to 1584 $cm^{-1}$ for sample exfoliated from EHOPG12 [50]. The

intensity ratio of P1 to P2 can be related to the intercalation stage index n denoting the number of graphitic layers between adjacent intercalate layers [19]. Therefore, the intercalation index for EHOPG3 sheets is n=5 whereas for the EHOPG12 sheets it is n=9, which is in agreement with XRD results.

Based on P2 peak intensity it can be concluded that C-C $E_{2g}$ stretching vibrations between adjacent graphene layers are more pronounced than those inside the graphene layers. The P3 peak corresponds to the edge defects in graphene (designated as the D' peak in the graphene Raman spectrum). The presence of defects (P3 peak intensity-this peak is not completely resolved from G peak and can be observed only after spectra are fitted) is more intense in the EHOPG3.

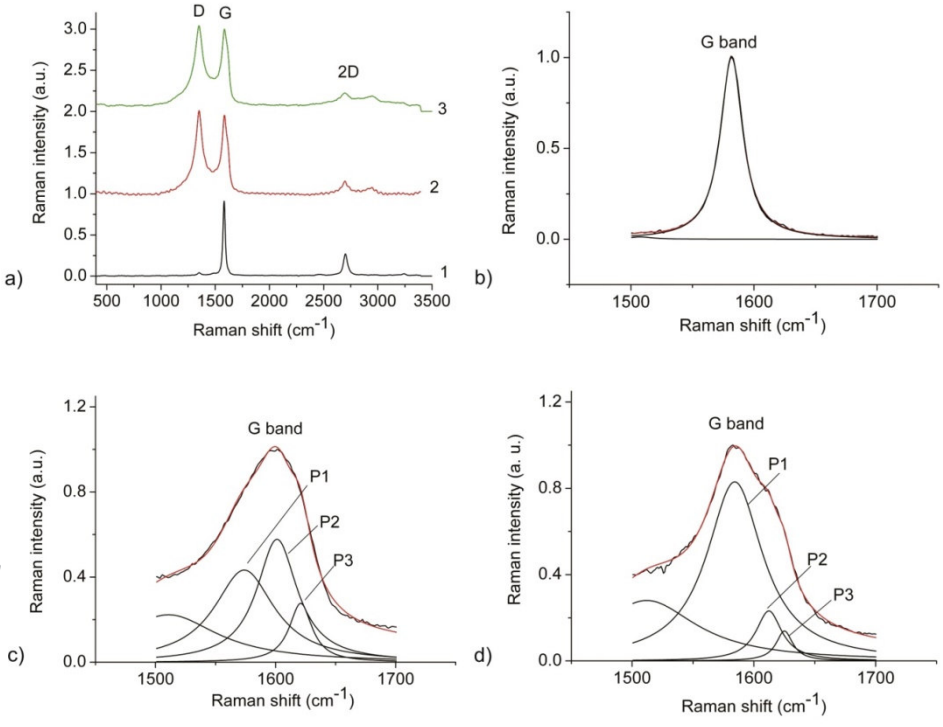

Fig. 4. a) Raman spectra of HOPG (curve 1), EHOPG3 (curve 2) and EHOPG12 (curve 3); b) Fitted Raman spectrum of HOPG, c) fitted Raman spectrum of EHOPG3 and d) fitted Raman spectrum of EHOPG12.

3.7. Electron paramagnetic resonance spectroscopy of EHOPG

It is known that graphene and GO generally are non-toxic for humans [51]. But it is found that reduced graphene oxide (rGO) generates ROS under visible light in air via a singlet oxygen–superoxide anion radical pathway [52]. Singlet oxygen is able to irreversibly cause damage of various cellular organelles and biomolecules, including mitochondria, lipids, and nucleus, thus leading to damage of cells or tissue [53].

EPR spectroscopy was used to determinate the ability of the EHOPG3 and EHOP12 samples to produce different reactive oxygen containing functional groups: singlet oxygen ($^1O_2$), hydroxyl ($HO^{\bullet}$) and superoxide radical ($O_2^{-\bullet}$).

To study the production of hydroxyl and superoxide radicals, we used DMPO as a spin trap [54]. First, we measured DMPO as a control experiment. These measurements were performed with and without light exposure and we noticed that there is no significant EPR signals-Figs. 5 (a, b). EPR measurements of samples mixed with DMPO did not show any differences compared to EPR spectrum of pure DMPO. After 10 minutes of light exposure, the production of hydroxyl and superoxide radicals cannot be detected-Fig. 5b.

The singlet oxygen production of studied dispersions was analyzed using a selective trap agent TEMP (Figs. 5 (c, d)) [55]. The technique is based on reaction between TEMP and singlet oxygen which leads to formation a stable, EPR active compound, 2,2,6,6-tetramethylpiperidine-1-oxyl (TEMPO). The singlet oxygen production in samples was also measured before and after photo-excitation.

We used EPR to obtain spectra of control TEMP solution and the EHOPG3 and EHOPG12 dispersions mixed with TEMP. All samples were recorded in dark (before light exposure) and after 10 minutes of illumination (Figs. 5 (c,d)). The control measurement of TEMP solution before light exposure showed a small TEMPO formation which can be ascribed to air exposure of TEMP during solution preparation. EPR spectra of samples mixed with TEMP in the absence of light do not show any significant changes in the intensity of signal characteristic for TEMPO compared to control measurement-Fig. 5c. After 10 minutes of light exposure, there is neither intensity increase of TEMPO signal for any of samples nor for the control experiment-Fig. 5d. Based on these analyses it can be concluded that the EHOPG3 and EHOPG12 do not produce singlet oxygen in dark or after 10 minutes of ligth exposure.

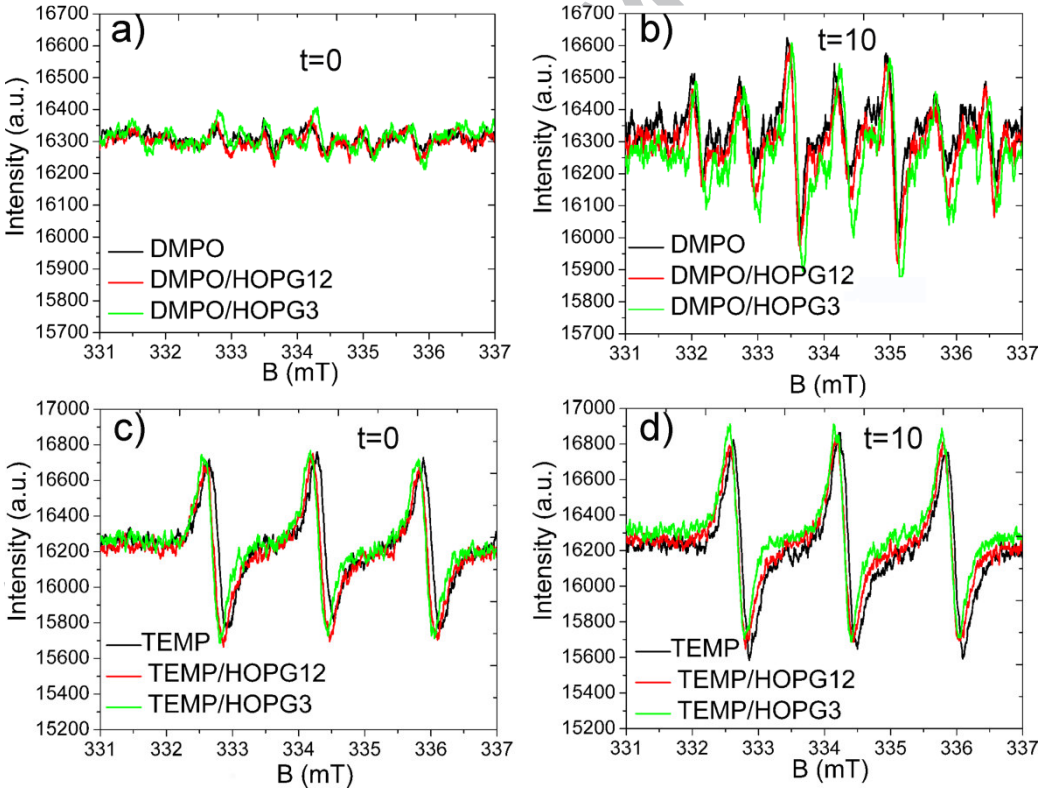

Fig. 5. a) EPR spectra of DMPO solution in dark conditions (t=0 min., black line), DMPO mixed with the EHOPG3 (t=0min., green curve); DMPO mixed with the EHOPG12 (t=0 min., red curve); b) EPR spectra of DMPO solution after 10 minutes of UV-light exposure (t=10 min., black curve), DMPO mixed with the EHOPG3 (t=10 min., green curve); DMPO mixed with the EHOPG12 (t=10 min., red curve); c) EPR spectra of TEMP solution in dark conditions (t=0 min., black line), TEMP mixed with the EHOPG3 (t=10 min., green curve), TEMP mixed with the EHOPG12 (t=10 min., red curve); d) EPR spectra of TEMP solution and after 10 minutes of UV-light exposure (t=10 min., black curve), TEMP mixed with the EHOPG3 (t=10 min., green curve); DMPO mixed with the EHOPG12 (t=10 min., red curve);

3.8. The antibacterial activity of EHOPG3 and EHOPG12

The effect of the EHOPG3 and EHOPG12 on the growth of *S. aureus* and *E. coli* was investigated. The growth curves of tested bacteria treated with different concentrations of exfoliated material (0.125–0.5 mg $mL^{-1}$), evaluated by measuring of $OD_{630}$, are shown in Figs. 6 (a–d). Due to the presence of the material that affects the interpretation of the data, the optical density of the bacteria cultures was corrected for $OD_{630}$ of sterile media with EHOPG3 and EHOPG12 at each time point. The standard deviation of all measured samples was 0.01 mg $mL^{-1}$. Material transformation was also observed in the inoculated media containing EHOPG3 and EHOPG12 with a change in the colour of the medium from light brown to dark brown and material precipitation by the end of incubation.

The growth curves of *S. aureus* treated with the different concentrations (0.125–0.5 mg $mL^{-1}$) of EHOPG3 (Fig. 6a) showed that its effect was neither inhibitory nor stimulatory. Even at the maximum tested concentration growth curves run parallel with that of the positive control and reached the same final $OD_{630}$. In the case of *S. aureus* treated with the EHOPG12 (Fig. 6c), a

bacterial growth phase was not detected when the concentration of 0.5 mg $mL^{-1}$ was used. The concentration 0.25 mg $mL^{-1}$ of EHOPG12 induced an extended lag phase and the attained OD630 value amounted to half of the maximum. *S. aureus* cells exposed to 0.125 mg $mL^{-1}$ of EHOPG12 were able to grow undisturbed.

The results of measuring of $OD_{630}$ showed that *E. coli* was able to grow in the presence of EHOPG3 (Fig. 6b) at the concentrations up to maximum tested – 0.5 mg $mL^{-1}$. In the case of *E. coli* treated with EHOPG12 (Figure 6d), the concentrations of 0.125 and 0.25 mg $mL^{-1}$ did not induce the inhibition of growth regarding control while treatment with 0.5 mg $mL^{-1}$ resulted in a lower final $OD_{630}$ value.

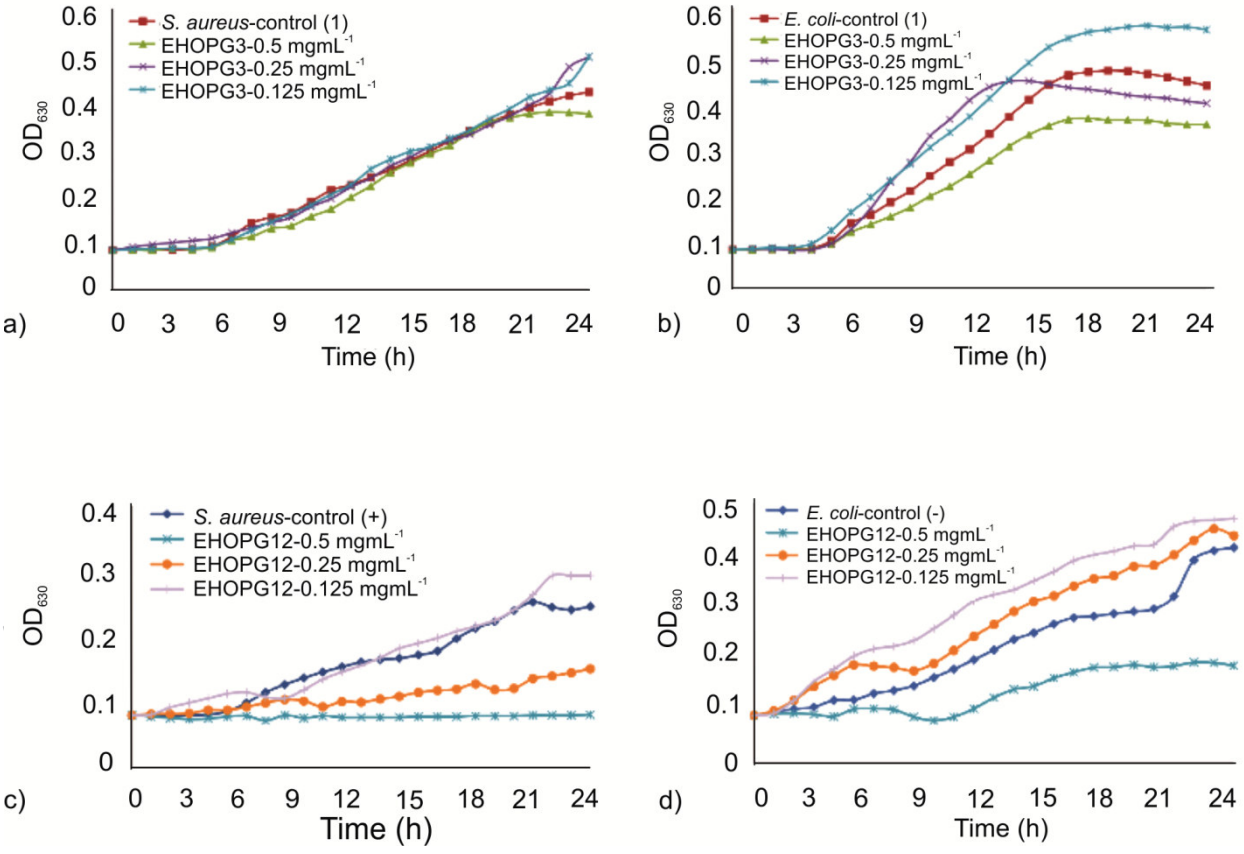

Fig. 6. Optical density of test culture in the media supplemented with: a) EHOPG3 at the concentration 0.125–0.5 mg $mL^{-1}$ – *S. aureus*, b) EHOPG3 at the concentration 0.125–0.5 mg $mL^{-1}$ – *E. coli*, c) EHOPG12 at the concentration 0.125–0.5 mg $mL^{-1}$ – *S. aureus* and d) EHOPG12 at the concentration 0.125–0.5 mg $mL^{-1}$ – *E. coli*.

Since the total number of bacteria, including live and dead ones, is assayed by $OD_{630}$, a decline phase could not be detected on the growth curves. Additionally, considering the difficulty in interpreting results due to precipitation of material, an alternative viable count assay was utilized. As shown in Table 4, treatment of *S. aureus* cells with 0.5 mg $mL^{-1}$ of EHOPG3 had no significant effect on bacterial growth while the same concentration of EHOPG12 evinced bacteriostatic activity. *E. coli* cells were able to grow in the presence of EHOPG3 and EHOPG12 at the concentration of 0.5 mg $mL^{-1}$, but the decline phase started earlier compared with the control.

Table 4. The antibacterial activity of the EHOPG3 and EHOPG12 expressed as log10 CFU $mL^{-1}$ determined by the broth macrodilution method.

*log10 CFU $mL^{-1}$

| Bacterial strain | 0 h | 3 h | 6 h | 9 h | 24 h |
|---|---|---|---|---|---|
| SAC | 5.0 ± 0.2a1 | 6.5 ± 0.2a | 7.2 ± 0.4a | 8.5 ± 0.4a | 8.8 ± 0.3a |
| SAEHOPG3 | 5.0 ± 0.1a | 6.5 ± 0.1a | 7.6 ± 0.4a | 7.8 ± 0.2a | 8.6 ± 0.5a |
| SAEHOPG12 | 4.9 ± 0.2a | 5.4 ± 0.2b | 5.2 ± 0.2b | 5.4 ± 0.2b | 5.7 ± 0.3b |

| | | | | | |
|---|---|---|---|---|---|
| ECC | 5.3 ± 0.3a | 7.0 ± 0.5a | 8.6 ± 0.3a | 8.7 ± 0.3a | 9.9 ± 0.6a |
| ECEHOPG3 | 5.3 ± 0.2a | 6.5 ± 0.3a | 8.5 ± 0.2a | 8.5 ± 0.4a | 8.1 ± 0.2b |
| ECEHOPG12 | 5.4 ± 0.3a | 6.3 ± 0.1a | 7.7 ± 0.2a | 8.0 ± 0.2a | 7.2 ± 0.2c |

C – control, log10 CFU $mL^{-1}$ without EHOPG3 and EHOPG12.

* Data are expressed as mean ± standard deviation (n = 3).

[1] Within the same column, means followed by different letters are significantly different at $\alpha$ = 0.05 (ANOVA, Tukey's HSD test).

3.9. Loss of 260-nm-absorbing material

The presence of materials, in cell free medium, that absorb at 260 nm indicate that large molecules (e.g. nucleic acids) have been lost from the cell interior and that major membrane damage has occurred. The $OD_{260}$s values of the filtrates from *S. aureus* and *E. coli* control suspensions remained approximately the same after 4 h as well as after 8 h. The $OD_{260}$s of the filtrates from *S. aureus* and *E. coli* suspensions treated with 0.5 mg $mL^{-1}$ of EHOPG3 or EHOPG12 also remained almost the same during the whole assay period (Fig. 7).

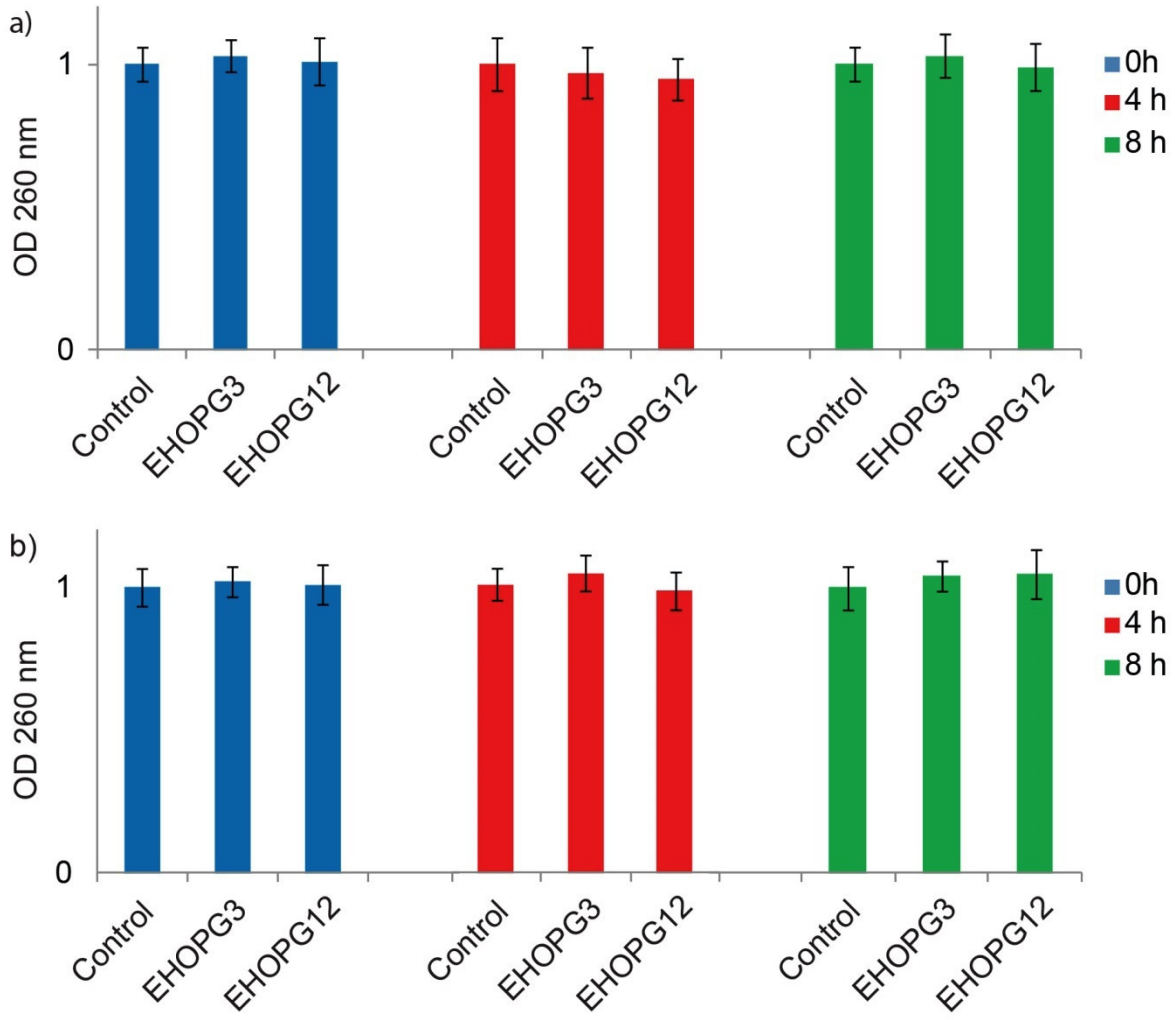


Fig. 7. Presence of 260-nm-absorbing material in the filtrates of: a) *S. aureus* after treatment with EHOPG3 and EHOPG12 at 4 and 8 h, compared to *S. aureus* control suspension and b) *E. coli* after treatment with EHOPG3 and EHOPG12 at 4 and 8 h, compared to *E. coli* control suspension. The mean ± SD for three replicates are illustrated.

3.10. Morphology of bacteria strains

Figs. 8 (a–c) present surface morphology of ECC, ECEHOPG3 and ECEHOPG12 samples whereas Figs. 8 (d–f) present the corresponding EDS spectra of these samples. As we can see from Fig. 8a average lengths of *E. coli* strains are 2 μm. In Fig. 8b we can not detect any changes

on bacteria membranes after interaction with the EHOPG3 whereas in Fig. 8c we can see neglectable damage of bacteria membranes during interaction with the EHOPG12. Based on a few SEM micrographs we calculated volumes of all microbes according to ref [56]. Data of average widths, lengths and volumes are presented in Table 5. Based on the presented data we can conclude that the volume value of the ECEHOPG12 differs from that of ECC. This value may indicate that the begining of exponential phase of *E. coli* cells treated with the EHOPG12 was a bit postponed. The EDS distributions of elements on untreated bacteria membranes have shown homogenious distributions of C, O, Na and P on bacteria membrane – Fig. 8d. After interaction with EHOPG, distributions of certain elements have been changed. The EDS qualitative analyses of ECC, ECEHOPG3 and ECEHOPG12 samples presented in Table 6 have shown that the content of C has slightly changed; content of O has almost raised twice, content of Na is the same whereas there is no trace of P after interaction with the EHOPG3 and EHOPG12. Fagerbakke et al. detected higher O:C ratio in small *E. coli* bacteria compared with larger ones [56]. These observations are in accordance with the obtained value for the volume of ECEHOPG12. Complete absence of P on bacteria membrane after interaction with the EHOPG3 and EHOPG12 may indicate leaking of intracellular substances or phosphorus is metabolized into other phosphates. But based on results presented in the section 3.9 it is indicative that phosphorus is metabolized into other phosphates hardly detectable by EDS [57].

Figs. 9 (a–c) present SEM micrographs of surface morphology of SAC, SAEHOPG3 and SAEHOPG12 samples whereas Figs. 9 (d–f) present the corresponding EDS distributions of elements detected on bacteria membranes. As can be seen from Fig. 9a average diameter of *S. aureus* is 500 nm. In Fig. 9b one can observe that EHOPG sheets tend to wrap bacteria strains aggregates whereas in Fig. 9c we can detect small damages on bacteria membranes. Based on

calculated parameters presented in Table 5 we can notice that there is volume change of SAEHOPG12 samples compared to SAC. Previous reports showed that *S. aureus* cells increased their volume continously throughout the entire cell cycle, from the volume 0.47 $\mu m^3$ at the begining to volume 0.91 $\mu m^3$ at the end of cycle [58]. In our experiment, samples were incubated for eight hours before they were subjected to EDS analysis. By that time, SAC cells entered the exponential phase and the assumption is that their volume increased. In the meantime the volume of cells treated with the EHOPG12 remained the same. As determined by other methods, the growth phases of *S. aureus* cells treated with EHOPG12 were not detected. Based on these results, the increase in volume of *S. aureus* was not expected. The EDS distribution of detected elements is homogenious only on untreated *S. aureus* whereas there are some changes in distribution of elements of treated bacteria. Table 6 presents changes of contents of detected elements on bacteria membranes. Significantly higher contents of P and O were detected in exponential phase of growth compared to stationary phase [56], which indicates that the amount of these elements changes during the life cycle of bacteria. Considering that the contents of P and O were almost two times higher in SAC and SAEHOPG3 than in SAEHOPG12, it can be concluded that *S. aureus* cells were captured in different stages of growth. Unlike the control and cells treated with EHOPG3, it seems that *S. aureus* cells treated with EHOPG12 did not enter the exponential phase of growth.

Table 5. Average widths, lengths, diameters and volumes of ECC, ECEHOPG3, ECEHOPG12, SAC, SAEHOPG3 and SAEHOPG12 samples.

| | ECC | ECEHOPG3 | ECEHOPG12 | SAC | SAEHOPG3 | SAEHOPG12 |
|---|---|---|---|---|---|---|
| Width(μm) | 0.6 | 0.6 | 0.5 | - | - | - |
| Length (μm) | 1.9 | 1.8 | 1.7 | - | - | - |
| Diameter (μm) | - | - | - | 1.01 | 0.97 | 0.85 |
| Volume ($\mu m^3$) | 1.14 | 0.86 | 0.86 | 0.54 | 0.48 | 0.32 |

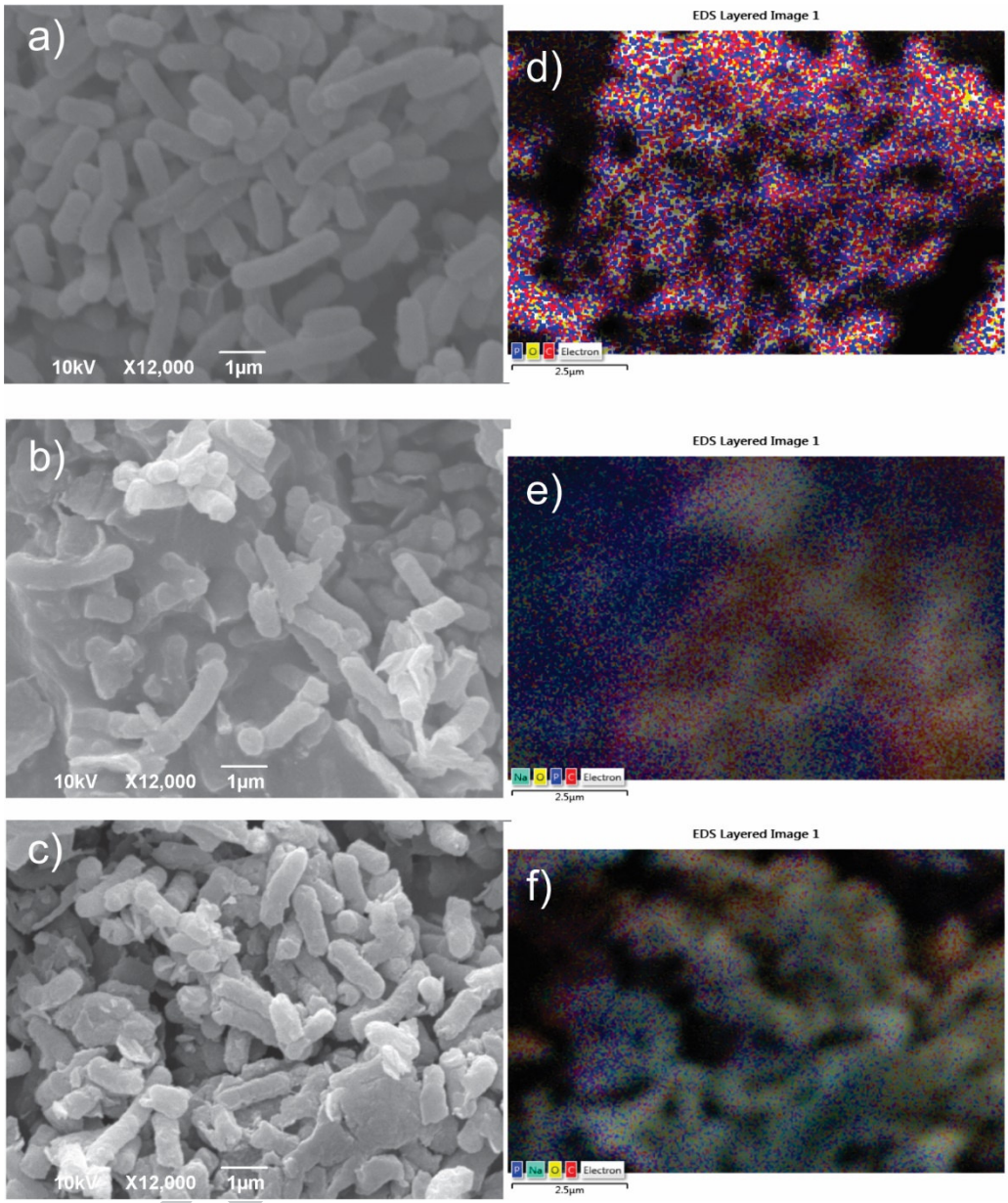


Fig. 8. SEM micrographs of a) ECC, b) ECEHOPG3, c) ECEHOPG12 samples and the corresponding EDS distribution of detected elements over the scanned area of the sample (d–f).

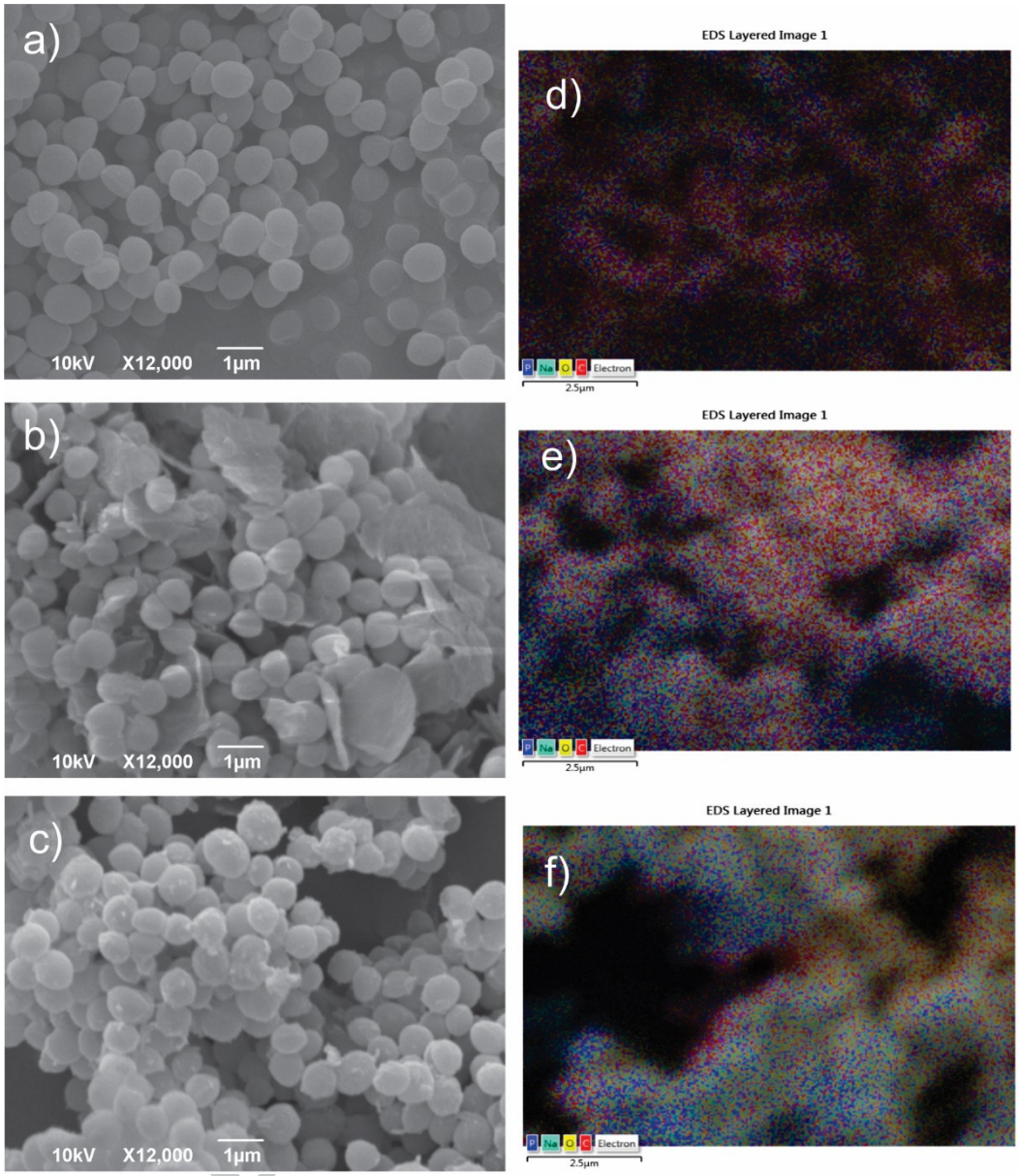


Fig. 9. SEM micrographs of a) SAC, b) SAEHOPG3, c) SAEHOPG12 samples and the corresponding EDS distribution of detected elements over the scanned area of the sample (d–f).

Table 6. The EDS distributions of detected elements over the scanned area of the sample in Wt %.

| | C | P | Na | O | P:C | O:C |
|---|---|---|---|---|---|---|
| ECC | 97.11 | 0.63 | - | 2.25 | 0.006 | 0.02 |
| ECEHOPG3 | 95.10 | - | 0.63 | 4.27 | - | 0.04 |
| ECEHOPG12 | 92.41 | - | 1.30 | 6.29 | - | 0.07 |
| SAC | 82.45 | 2.88 | 2.47 | 12.20 | 0.03 | 0.15 |
| SAEHOPG3 | 80.47 | 2.98 | 3.16 | 13.39 | 0.04 | 0.17 |
| SAEHOPG12 | 90.37 | 1.79 | 2.27 | 5.58 | 0.02 | 0.06 |

## 4. DISCUSSION

Antibacterial activities of two water dispersible graphene derivatives were tested in this study. Commonly tested features of material that influence antibacterial response are: chemical composition, redox potential, surface charge, hydrophobicity, surface roughness, surface topography and surface to volume ratio [59]. Despite of the fact that both electrochemically exfoliated graphene derivatives are electrically conducting [19], have different lateral size and thickness of sheets, surface charge, sulfur content and degree of defects, antibacterial effect is very poor for both materials.

The EHOPG3 sample has almost two times larger and four times thinner sheets than the EHOPG12. But antibacterial analysis has not shown that surface to volume ratio affects significantly bacterial activity. We only observed that *S. aureus* cells entrapped in the larger EHOPG3 sheets (Fig. 9b). We could not detect any significant damage on bacteria membrane or cell growth inhibition by exfoliated sheets embedding. That effect was not observed during interaction of *S. aureus* with the EHOPG12. As for concentration of samples it was established that treatment of *S. aureus* cells with 0.5 mg $mL^{-1}$ of the EHOPG3 had no significant effect on bacterial growth while the same concentration of the EHOPG12 evinced bacteriostatic activity. *E. coli* cells were able to grow in the presence of the EHOPG3 and EHOPG12 at the concentration of 0.5 mg $mL^{-1}$, but the decline phase started earlier compared to the control. Both samples have similar values of rms surface roughness. Although the EHOPG3 sample has higher hydrophobicity compared to the EHOPG12 sample results of antibacterials tests did not confirm assumptions that bacterial cells have higher affinity for hydrophobic surfaces due to hydrophobic interactions, which depends on the type of bacteria tested [59]. Therefore, the EHOPG3 sample has neither inhibitory nor stimulatory effect on *S. aureus* growth. As for *E. coli*, these bacteria were able to grow in the presence of the EHOPG3 and EHOPG12 at the concentration of 0.5 mg $mL^{-1}$.

Current explanations of antibacterial activity of graphene based materials [25, 26] based on redox potential of graphene and sharp edge effect of graphene oxide sheets, can not explain results of this study. The first mechanism based on redox potential of conductive graphene sheet catalyzes production of reactive oxygen species. ROS damage the membrane and such effect was not detected on SEM images. Furthermore, our water dispersible graphene derivatives functionalized with carboxyl and hydroxyl groups similar to functionalized relative fullerene,

will quickly quench any ROS [60]. The second explanation based on mechanistic approach, i.e. cutting of bacteria with sharp edges of functionalized graphene can not be applied for results of our study, despite of the fact that we have graphenes with very large aspect ratio (diameter/height=11500). High values of zeta potential of graphene derivatives ensure lack of agglomeration in presence of bacteria and maintaining of sharp graphene edges. The third option for antibacterial activity is dissolution of phospholipid by graphene which can occur if surface energies are similar. However since surface energy of bacteria is three times larger that surface energy of graphene derivatives, explanation on solubility is not viable. The fourth explanation for antibacterial activity of GO is high level of sulfur impurities. Barbolina et al. [32] have shown that GO with sulfur content over 1.7 % has antibacterial effect contrary to GO with smaller amount of sulfur. Although in our study, content of sulfur in EHOPG3 was 2.3 %, we have not detected any antibacterial activity. Our pH neutral graphene derivatives have intercalated sulfur (trapped between layers) unlike GO, so sulfur ions were not in direct contact with bacteria membrane.

Sole detectable effect of interaction between graphene derivatives and bacteria is the presence of phosphorus from bacteria membrane on graphene sheets. But loss of 260-nm-absorbing material method has shown that the $OD_{260}$s of the filtrates from *S. aureus* and *E. coli* suspensions treated with 0.5 mg $mL^{-1}$ of EHOPG3 or EHOPG12 remained almost the same during the whole assay period. Considering that the contents of P and O were almost two times higher in SAC and SAEHOPG3 than in SAEHOPG12, it can be concluded that *S. aureus* cells were captured in different stages of growth. This is an indication that phosphorus is metabolized into other phosphates and bacteria membrane is not damaged. Bacteria managed to reorganize its membrane in such way to survive even in the presence of the largest concentrations of graphene

derivatives. This effect is more pronounced in the case of *S. aureus*. EDS images (Figs. 9 (e,f)) indicate lack of phosphorus on sites where *S. aureus* are accumulated (Fig. 9c-left side) or increased level of phosphorus on sites where EHOPG3 sheets are located (Fig. 9e-right upper corner).

## 5. CONCLUSION

Despite initial enthusiasm about potential use of graphene as antibacterial agent, the progress in their development is still in its infancy. One of the main reasons is an inadequate understanding of graphene structure - antibacterial function correlation with respect to different modifications required to provide water dispersibility. There is a huge disagreement in scientific community about dominant mechanism of graphene toxicity or lack of it.

In this paper we have characterized in detail all features of the EHOPG sheets obtained electrochemically from HOPG that might be responsible for its antibacterial activity. Although EHOPG sheets were able to perform redox reactions like antibacterial metal dots and were sharp enough for edgewise contact, we have not noticed significant antibacterial activity against *S. aureus* and *E. coli*. Based on loss of 260-nm-absorbing material method it was found that large molecules (e.g. nucleic acids) have not been lost from the cell interior. The variation of P and O contents of membrane during interaction of *E. coli* and *S. aureus* with the EHOPG3 and EHOPG12 was found. Significantly higher contents of P and O were detected in the exponential phase of growth compared to stationary phase which indicates that the amount of these elements changes during the life cycle of bacteria.

The contradictory explanations regarding the bactericidal properties of graphene can be ascribed to the variations in the physicochemical features for each individual sample. In the future work,

some kind of modifications of graphene must be applied (i.e.functionalization with metal nanoparticles with strong antibacterial properties) to enhance its poor antibacterial activity.

Acknowledgements

This research was supported by the SASPRO Programme project 1237/02/02-b. The research leading to these results has received funding from the People Programme (Marie Curie Actions) European Union's Seventh Framework Programme under REA grant agreement No. 609427. Research has been further co-funded by the Slovak Academy of Sciences. Research was also supported by the Ministry of Education, Science and Technological Development of the Republic of Serbia (project no. 172003 and III 46010), bilateral project Serbia-Slovakia SK-SRB-2016-0038, multilateral scientific and technological cooperation in the Danube region (DS021) and VEGA (2/0093/16). Mrs. Marcela Kimlickova is gratefully acknowledged for performing zeta potential measurements.

References

[1] K. S. Novoselov, A. K. Geim, S. V. Morozov, D. Jiang, Y. Zhang, S. V. Dubonos, I. V. Grigorieva, A. A. Firsov, Electric field effect in atomically thin carbon films, Science 306 (2004) 666–669.

[2] S. Bae, H. Kim, Y. Lee, X. Xu, J. S. Park, Y. Zheng, J. Balakrishnan, T. Lei, H. R. Kim, Y. I. Song, Y. J. Kim, K. S. Kim, B. Özyilmaz, J. H. Ahn, B. H. Hong, S. Iijima, Roll-to-roll production of 30-inch graphene films for transparent electrodes, Nat. Nanotechnol. 5 (2010) 574–578.

[3] K. Chen, S. Song, F. Liua, D. Xue, Structural design of graphene for use in electrochemical energy storage devices, Chem. Soc. Rev. 44 (2015) 62306257.

[4] F. Liu, S. Song, D. Xue, H. Zhang, Folded Structured Graphene Paper for High Performance Electrode Materials, Adv. Mater. 24 (2012) 1089–1094.

[5] K. Chen, D. Xue, S. Komarneni, Colloidal pseudocapacitor: Nanoscale aggregation of Mn colloids from $MnCl_2$ under alkaline condition, J. Power Sources 279 (2015) 365–371.

[6] C. Chung, Y. K. Kim, D. Shin, S. R. Ryoo, B. H. Hong, D. H. Min, Biomedical applications of graphene and graphene oxide, Acc. Chem. Res. 46 (2013) 2211–2224.

[7] S. Szunerits, R. Boukherroub, Antibacterial activity of graphene-based materials, J. Mater. Chem. B 4 (2016) 6892–6912.

[8] J. Liu, C. K. Poh, D. Zhan, L. Lai, S. H. Lim, L. Wang, X. Liu, N. G. Sahoo, C. Li, Z. Shen, J. Lin, Improved synthesis of graphene flakes from the multiple electrochemical exfoliation of graphite rod, Nano Energy 2 (2013) 377–386.

[9] M. Zhou, J. Tang, Q. Cheng, G. Xu, P. Cui, L. Qin, Few-layer graphene obtained by electrochemical exfoliation of graphite cathode, Chem. Phys. Lett. 572 (2013) 61–65.

[10] A. Reina, X. Jia, J. Ho, D. Nezich, H. Son, V. Bulovic, M. S. Dresselhaus, J. Kong, Large Area, Few-layer graphene films on arbitrary substrates by chemical vapor deposition, Nano Lett. 9 (2008) 30–35.

[11] S. Lee, K. Lee, Z. Zhong, Wafer scale homogeneous bilayer graphene films by chemical vapor deposition, Nano Lett. 10 (2010) 4702–4707.

[12] P. W. Sutter, J. I. Flege, E. A. Sutter, Epitaxial graphene on ruthenium, Nat. Mater. 7 (2008) 406–411.

[13] W. Hummers, R. Offeman, Preparation of graphitic oxide, J. Am. Chem. Soc. 80 (1958) 1339.

[14] K. Parvez, Z. S. Wu, R. Li, X. Liu, R. Graf, X. Feng, K. Müllen, Exfoliation of graphite into graphene in aqueous solutions of inorganic salts, J. Am. Chem. Soc. 136 (2014) 6083−6091.

[15]K. Chen, D. Xue, Preparation of colloidal graphene in quantity by electrochemical exfoliation, J. Colloid Interface Sci. 436 (2014) 41−46.

[16] K. Chen, D. Xue, S. Komarneni, Nanoclay assisted electrochemical exfoliation of pencil core to high conductive graphene thin-film electrode, J. Colloid Interface Sci. 487 (2017) 156−161.

[17] K. Chen, D. Xue, In-situ electrochemical route to aerogel electrode materials of graphene and hexagonal $CeO_2$, J. Colloid Interface Sci. 446 (2015) 77−83.

[18] M. Coros, F. Pogacean, M. C. Rosu, C. Socaci, G. Borodi, L. Magerusan, A. R. Biris, S. Pruneanu, Simple and cost-effective synthesis of graphene by electrochemical exfoliation of graphite rods, RSC Adv. 6 (2016) 2651–2661.

[19] Z. M. Marković, M. D. Budimir, D. P. Kepić, I. D. Holclajtner-Antunović, M. D. Dramićanin, V. D. Spasojević, D. B. Peruško, Z. Špitalský, M. Mičušik, V. B. Pavlović, B. M. Todorović-Marković, Study of semi-transparent, conductive thin films of electrochemical exfoliated graphene, RSC Adv. 6 (2016) 39275–39283.

[20] A. Bianco, H. M. Cheng, T. Enoki, Y. Gogotsi, R. H. Hurt, N. Koratkar, T. Kyotani, M. Monthioux, C. R. Park, J. M. D. Tascon, J. Zhang, All in the graphene family- a recommended nomenclature for two-dimensional carbon materials, Carbon 65 (2013) 1–6.

[21] A. C. Ferrari, J. C. Meyer, V. Scardaci, C. Casiraghi, M. Lazzeri, F. Mauri, S. Piscanec, D. Jiang, K. S. Novoselov, S. Roth, A. K. Geim, Raman spectrum of graphene and graphene layers, Phys. Rev. Lett. 97 (2006) 187401.

[22] Z. Y. Xia, S. Pezzini, E. Treossi, G. Giambastiani, F. Corticelli, V. Morandi, A. Zanelli, V. Bellani, V. Palermo, The exfoliation of graphene in liquids by electrochemical, chemical, and sonication-assisted techniques: A nanoscale study, Adv. Funct. Mater. 23 (2013) 4684–4693.

[23] O. Akhavan, E. Ghaderi, Toxicity of graphene and graphene oxide nanowalls against bacteria, ACS Nano 4 (2010) 731−736.

[24] W. Hu, C. Peng, W. Luo, M. Lv, X. Li, D. Li, Q. Huang, C. Fan, Graphene-based antibacterial paper, ACS Nano 4 (2010) 4317−4323.

[25] J. Li, G. Wang, H. Zhu, M. Zhang, X. Zheng, Z. Di, X. Liu, X. Wang, Antibacterial activity of large-area monolayer graphene film manipulated by charge transfer, Sci. Rep. 4 (2014) 4359.

[26] L. Hui, J. G. Piao, J. Auletta, K. Hu, Y. Zhu, T. Meyer, H. Liu, L. Yang, Availability of the basal planes of graphene oxide determines whether it is antibacterial, ACS Appl. Mater. Interfaces 6 (2014) 13183−13190.

[27] O. Akhavan, E. Ghaderi, Escherichia coli bacteria reduce graphene oxide to bactericidal graphene in a self-limiting manner, Carbon 5 (2012) 1853−1860.

[28] S. Liu, M. Hu, T. H. Zeng, R. Wu, R. Jiang, J. Wei, L. Wang, J. Kong, Y. Yuan Chen, Lateral dimension-dependent antibacterial activity of graphene oxide sheets, Langmuir 28 (2012) 12364−12372.

[29] J. Zhao, B. Deng, M. Lv, J. Li, Y. Zhang, H. Jiang, C. Peng, J. Li, J. Shi, Q. Huang, C. Fan, Graphene oxide-based antibacterial cotton fabrics, Adv. Healthcare Mater. 2 (2013) 1259–1266.

[30] M. C. Wu, A. R. Deokar, J. H. Liao, P. Y. Shih, Y. C. Ling, Graphene-based photothermal agent for rapid and effective killing of bacteria, ACS Nano 7 (2013) 1281–1290.

[31] O. N. Ruiz, K. A. Shiral Fernando, B. Wang, N. A. Brown, P. G. Luo, N. D. McNamara, M. Vangsness, Y. P. Sun, C. E. Bunker, Graphene oxide: a nonspecific enhancer of cellular growth, ACS Nano 5 (2011) 8100–8107.

[32] I. Barbolina, C. R. Woods, N. Lozano, K. Kostarelos, K. S. Novoselov, I. S. Roberts, Purity of graphene oxide determines its antibacterial activity, 2D Materials 3 (2016) 1–12.

[33] H. M. Hegab, A. ElMekawy, L. Zou, D. Mulchahy, C. P. Saint, M. Ginić Marković, The controversial antibacterial activity of graphene-based materials, Carbon 105 (2016) 362–376.

[34] S. M. Notley, R. J. Crawford, E. P. Ivanova, Bacterial interaction with graphene particles and surfaces, in: M. Aliofkhazraei (Ed.), Advances in Graphene Science, InTech., 2013, pp. 100–118. DOI: 10.5772/56172. Available from:

http://www.intechopen.com/books/advances-in-graphene-science/bacterial-interaction-with-graphene-particles-and-surfaces.

[35] B. Todorović Marković, S. Jovanović, V. Jokanović, Z. Nedić, M. Dramićanin, Z. Marković, Atomic force microscopy study of fullerene-based colloids, Appl. Surf. Sci. 255 (2008) 3283–3288.

[36] www.gwyddion.net. Version 2.42.

[37] F. Garbassi, M. Morra, E. Occhielo, Polymer surfaces from physics to technology, 1994.

[38] S. M. Pawde, K. Deshmukh, Surface characterization of air plasma treated poly vinylidene fluoride and poly methyl methacrylate films, Polym. Eng. Sci. 49 (2009) 808–818.

[39] F. Widdel, Theory and measurement of bacterial growth. Grundpraktikum Mikrobiologie, Universität Bremen 4 (2007) 11.

[40] A. Klančnik, S. Piskernik, B. Jeršek, S. S. Možina, Evaluation of diffusion and dilution methods to determine the antibacterial activity of plant extracts, J. Microbiol. Methods 81 (2010) 121–126.

[41] C. F. Carson, B. J. Mee, T. V. Riley, Mechanism of action of Melaleuca alternifolia (tea tree) oil on Staphylococcus aureus determined by time-kill, lysis, leakage, and salt tolerance assays and electron microscopy. Antimicrob. Agents Chemother. 46 (2002) 1914–1920.

[42] A. K. Tyagi, D. Bukvički, D. Gottardi, M. Veljić, M. E. Guerzoni, A. Malik, P. D. Marin, Antimicrobial potential and chemical characterization of serbian liverworth (porella arboris-vitae): sem and tem observation, Evid. Based Complement Altern. Med. 2013.

Available from:

https://www.hindawi.com/journals/ecam/2013/382927/abs/(DOI:10.1155/2013/382927).

[43] XPS knowledge database, Avantage 5.955, Thermo Fisher Scientific, UK.

[44] XPS of Polymers Database, Eds. G. Beamson&D. Briggs, Surface Spectra Ltd., ISBN 0-9537848-4-3.

[45] H. Busscher, A. Weercamp, H. C. J. der Mei, A. W. van Pelt, H. P. Jong, J. Arends, Measurement of the surface free energy of bacterial cell surfaces and its relevance for adhesion, Appl. Environ. Microbiol. 48 (1984) 980–983.

[46] A. Jillavenkatesa, S. J. Dapkaunas, L. H. Lum, Particle size characterization, Natl. Inst. Stand. Technol. Spec. Publ. 960-1 (2001) 960–961.

[47] S. C. Jun, Fundamental of graphene, in: A. Rashid bin Mohd Yusof (Ed.), Graphene-based energy devices, Wiley-VCH Verlag GmbH&Co. KGaA, 2015, pp. 1–48.

[48] L. M. Malard, M. A. Pimenta, G. Dresselhaus, M. S. Dresselhaus, Raman spectroscopy in graphene, Phys. Rep. 473 (2009) 51–87.

[49] A. C. Ferrari, Raman spectroscopy of graphene and graphite: disorder, electron-phonon coupling, doping and non-adiabatic effects, Solid State Commun. 14 (2007) 47−57.

[50] M. S. Dresselhaus, G. Dresselhaus, Intercalation compounds of graphite, Adv. Phys. 5 (2002) 1−186.

[51] M. Saxena and S. Sarkar, Involuntary graphene intake with food and medicine, RSC Adv. 4 (2014) 30162–30167.

[52] T. Dutta, R. Sarkar, B. Pakhira, S. Ghosh, R. Sarkar, A. Barui, S. Sarkar, ROS generation by reduced graphene oxide (rGO) induced by visible light showing antibacterial activity: comparison with graphene oxide (GO)†, RSC Adv. 5 (2015) 80192–80195.

[53] M. J. Ochsner, Photophysical and photobiological processes in photodynamic therapy of tumors, J. Photochem. Photobiol. B 39 (1997) 1–18.

[54] G. R. Buettner, The spin trapping of superoxide and hydroxyl free radicals with DMPO (5,5-dimethylpyrroline-N-oxide): more about iron, Free Radic Res Commun. 19 (1993) Suppl. 1 S79-87.

[55] Y. Lion, M. Delmelle, A. Van de Vorst, New method of detecting singlet oxygen production, Nature 263 (1976) 442–443.

[56] K. M. Fagerbakke, M. Heldal, S. Norland, Content of carbon, nitrogen, oxygen, sulfur and phosphorus in native aquatic and cultured bacteria, Aquat. Microb. Ecol. 10 (1996) 15–27.

[57] H. E. Wade, Variation in the Phosphorus Content of Escherichiu coli during Cultivation (1952) J. Gen. Microbiol. 7 (1952) 24–30.

[58] J. M. Monteiro, P. B. Fernandes, F. Vaz, A. R. Pereira, A. C. Tavares, M. T. Ferreira, M. G. Pinho, Cell shape dynamics during the staphylococcal cell cycle, Nat. Commun. 6 (2015) 8055.

[59] A. Krasowska, K. Sigler How microorganisms use hydrophobicity and what does this mean for human needs? Front. Cell. Infect. Microbiol. 4 (2014) 112.

[60] Z. Marković, V. Trajković, Biomedical potential of the reactive oxygen species generation and quenching by fullerenes ($C_{60}$), Biomaterials 29 (2008) 3561–3573.

**Graphical abstract**